Doubly shaped D_2 excitation spectra of Cs and Rb atoms in superfluid helium due to a quadrupole bubble surface oscillation

T. Kinoshita,* K. Fukuda, and T. Yabuzaki
Department of Physics, Faculty of Science, Kyoto University, Kyoto 606-01, Japan
(Received 22 September 1995; revised manuscript received 8 April 1996)

Our recent experiments show that the D_2 excitation spectra of Cs and Rb atoms in superfluid helium have doubly shaped profiles. Such line shapes are beyond the description of a simplified spherical atomic bubble model which explains properly general features of optical spectra of neutral atoms in liquid helium. This paper gives a theoretical explanation of the doubly shaped profiles, with a model that the bubble structure of surrounding helium is not spherical, but is deformed instantaneously by a quadrupole oscillation. The calculated energy level of the $P_{3/2}$ state of the deformed atomic bubble is split into two branches, giving the D_2 excitation line shape consisting of two components with different peak intensities and widths. The obtained line shape agrees qualitatively with the observed one, which enables us to confirm the importance of the dynamic Jahn-Teller effect due to a quadrupole oscillation of the atomic bubble surface induced by zero-point fluctuations. [S0163-1829(96)06633-7]

I. INTRODUCTION

The spectral structures and broadening of impurity atoms and ions in condensed matter are strongly affected by collective oscillations of lattices or surrounding media. The optical properties and the dynamics of impurities in solids have been interpreted with configuration coordinate diagrams thus far. Franck-Condon factors for a transition between vibronic states in electronic ground and excited states determine the optical line shape and broadening, which give us important information about the interaction between the impurity and surrounding media. Among a large number of lattice vibrations, some oscillation modes accompanying the distortion of surrounding media result in a reduction of symmetry of the potential for an impurity center, and cause sometimes splitting in optical spectra. For example, alkali metal and alkaline earth atoms in rare gas matrices are known to have multiple splitting structures in the optical absorption and excitation spectra.[1,2] Various explanations have been given for these line shapes, and recent results of a magnetic circular dichroism (MCD) experiment suggest the importance of the Jahn-Teller effect.[2]

In recent years, the optical properties of neutral atoms immersed in superfluid helium (He II) have been studied extensively, both experimentally and theoretically.[3–11] It is well known that neutral atoms in liquid helium form bubbles (atomic bubbles) and are self-trapped therein due to the Pauli repulsive force between valence electrons of the impurity and of surrounding helium atoms. The bubble radius is about the same as the size of an impurity atom, which is in good contrast to the electron bubble having a much larger radius, typically, 15–25 Å.[12–16]

Recently we observed D_1, D_2 excitation ($5^2S_{1/2} \rightarrow 5^2P_{1/2}$, $5^2P_{3/2}$, $6^2S_{1/2} \rightarrow 6^2P_{1/2}$, $6^2P_{3/2}$) and D_1 emission ($5^2P_{1/2} \rightarrow 5^2S_{1/2}$, $6^2P_{1/2} \rightarrow 6^2S_{1/2}$) spectra of alkali metal atoms (Rb and Cs) in He II, respectively, changing the helium pressure from saturated vapor pressure (SVP, 7.4×10^{-3} atm) to about 25 atm. To explain the features of the observed spectra, we carried out theoretical calculations with a spherical bubble model (SBM).[10,11] In this model, the bubble radius R_0 corresponds to the configuration coordinate, which is analogous to the internuclear distance of diatomic molecules. We calculated the adiabatic potentials of the ground and excited states of a spherical atomic bubble, taking account of only breathing modes among various bubble surface oscillation modes. Namely, we neglected the effect of distortion of the bubble shape on the optical transitions. Using this simplified bubble model, we could reproduce qualitatively the general features of the observed spectra (pressure shift and broadening, and line shape of the D_1 lines) of Rb and Cs atoms.

On the other hand, the observed D_2 excitation spectrum has a double-peak structure.[10] The spectrum is comprised of two components, the broader one located on the side of shorter wavelength and the sharper one at the longer wavelength. The line shape was found to be well fit to the sum of two Gaussian curves. The splitting interval of the Cs-D_2 line, for example, is 122.1 cm^{-1} at SVP and 157.0 cm^{-1} at 20 atm, depending slightly on the helium pressure ($\sim$1.6 cm^{-1}/atm). The sharper line is stronger than the other, and the relative peak intensities are $\sim$ 1 : 1.5. A similar line shape has already been reported in the case of the D_2 excitation transition from the ground state $6^2S_{1/2}$ to the excited $6^2P_{3/2}$ state of Ba^+ ions in He II at SVP.[17] The line-splitting interval in this case was larger ($\sim$390 cm^{-1}) and the peak intensity of the line on the longer-wavelength side was about twice as large as the other line. These experimental facts are essentially beyond description within the framework of the spherical atomic bubble model, and suggest the importance of anisotropic bubble surface oscillations, causing the nontotally symmetric configuration of surrounding helium atoms. Among a large number of theoretical studies for various impurities in liquid helium based on the bubble model, some works have treated the effects of surface deformation of the atomic bubbles[5,8] and of the electron bubble.[12,16,18–20] However, such a structured shape of the excitation line has never been studied theoretically.

In the present work, we devote ourselves to understanding the physical mechanism to produce the structured line shape of the Cs-D_2 excitation spectra in liquid helium. We introduce a deformed atomic bubble model where the deformation is expressed by two parameters characterizing the quadrupole oscillation modes of the bubble surface. Two configuration coordinates with these two parameters are analogous to two normal coordinates giving the E_g vibrational modes for an atom trapped in a matrix with cubic symmetry. The preliminary result of calculation about the Cs-D_2 excitation line shape has already been reported.[11] In this paper we describe our theoretical model in detail including the quadrupole deformation of the bubble shape and present a qualitative explanation for the doubly shaped profile as the dynamic Jahn-Teller effect.

II. THEORETICAL MODEL

A. Basic description of the bubble model

We assume that an impurity atom in liquid helium forms a cavity of about atomic size (the atomic bubble model). The existence of such a stable cavity has been made clear in recent experimental and theoretical works. Let us consider the case of an alkali atom in liquid helium. We treat liquid helium as a continuously distributed medium. The density profile of helium atoms is denoted by $\rho(\mathbf{R})$, where $\mathbf{R}$ represents the position vector of the helium atom relative to the alkali nucleus. The total Hamiltonian to be diagonalized can be written as

$$H_E = H_A(r) + \int d\mathbf{R}\rho(R,\Theta,\Phi)\sum_{L=0}^{\infty} V_I^{(L)}(r,R) \times \frac{4\pi}{2L+1}\sum_{M=-L}^{L} Y_L^M{}^*(\theta,\phi)Y_L^M(\Theta,\Phi), \qquad (2.1)$$

where $\mathbf{r}$ is the position vector of the alkali metal valence electron relative to the alkali nucleus, and we have used the polar coordinates $\mathbf{r}=(r,\theta,\phi)$ and $\mathbf{R}=(R,\Theta,\Phi)$. $H_A(r)$ is the Hamiltonian for the valence electron of a free alkali metal atom including the spin-orbit interaction, and $V_I^{(L)}(r,R)$ is obtained by expanding the potential $V_I(\mathbf{r},\mathbf{R})$ in terms of the Legendre polynomials:

$$V_I^{(L)}(r,R) = \frac{2L+1}{2}\int_{-1}^{1} d(\cos\eta)V_I(\mathbf{r},\mathbf{R})P_L(\cos\eta). \qquad (2.2)$$

Here η is the angle between $\mathbf{r}$ and $\mathbf{R}$. $V_I(\mathbf{r},\mathbf{R})$ represents the sum of interactions between three bodies, the frozen alkali core, the frozen helium atom, and the alkali metal valence electron:[21,22]

$$V_I(\mathbf{r},\mathbf{R}) = F(\mathbf{r},\mathbf{R}) + G(\mathbf{r},\mathbf{R}) + W(R), \qquad (2.3)$$

where $F(\mathbf{r},\mathbf{R})$ is the effective electrostatic interaction between alkali metal and helium atoms. The terms $G(\mathbf{r},\mathbf{R})$ and $W(R)$ represent the pseudopotentials corresponding to the compensational energies arising due to the lack of orthogonality of the helium atom with the valence electron and the alkali core, respectively. Similar pseudopotential techniques were used extensively to calculate the electron-helium atom interaction in the case of the electron bubble.[13,14,23] The expressions for above three terms and the values for some parameters are given by Baylis[21] and Pascale and Vandeplanque.[22] Eigenenergies can be obtained by diagonalizing the Hamiltonian H_E in the unperturbed alkali atomic wave functions in the ground state and the first excited P states which are calculated by solving numerically the Schrödinger equation for the valence electron determined by the Hartree-Fock-Slater self-consistent field method under the frozen atomic core approximation.[24]

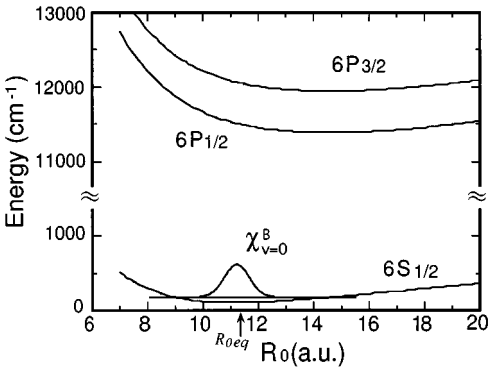

FIG. 1. The total energy diagram of the Cs atomic bubble in the $6S_{1/2}$, and $6P_{1/2}$ and $6P_{3/2}$ states at the SVP as functions of the spherical bubble radius R_0. The energy differences between the ground and excited states at $R_0=\infty$ are equal to that of a free Cs atom. The symbol $R_{0\mathrm{eq}}$ represents the equilibrium bubble radius in the ground state ($R_{0\mathrm{eq}}$ = 11.375 a.u.). These energy curves can be regarded as the adiabatic potentials, giving the quantized breathing modes of bubble surface oscillation.

In the case of the spherical bubble model (SBM), helium atoms are assumed to distribute isotropically outside the cavity of radius R_0 with the width at the cavity edge determined by a parameter α.[14] The equilibrium bubble radius $R_{0\mathrm{eq}}$ and the equilibrium value of α are determined by minimizing the total energy of this system:

$$E_{\mathrm{tot}}(R_0,\alpha) = E_{\mathrm{atom}} + 4\pi R_b^2\sigma + \frac{4}{3}\pi R_b^3 P + \hbar^2/(8M_{\mathrm{He}})\int d^3R(\nabla\rho)^2/\rho, \qquad (2.4)$$

where E_{atom} is the atomic energy in liquid helium given as the eigenenergy of Eq. (2.1). The other three terms in Eq. (2.4) represent the classical energies to form the cavity: the surface energy E_{surf}, the pressure volume work E_{PV}, and the volume kinetic energy E_{VK}.[14] In Eq. (2.4), P is the helium pressure, σ is the surface tension at 1.6 K,[25] which is assumed to be independent of the helium pressure, M_{He} is the mass of the helium atom, and R_b is the effective bubble radius defined by the ''center of mass'' in the region of the cavity edge.[5]

Figure 1 shows the total energies calculated with the SBM for the excitation from the $6S_{1/2}$ state to the $6P_{1/2}$ and $6P_{3/2}$ states of the Cs bubble at SVP. In the present work, the equilibrium bubble radius $R_{0\mathrm{eq}}$ in the ground state $S_{1/2}$ was calculated to be 11.375 a.u. at SVP and 10.975 a.u. at 20 atm. These calculated energy curves as functions of the con-

figuration coordinate R_0 are considered to be effective potentials for the quantized breathing oscillation of the bubble surface with an effective mass $M_{\rm eff}^B$ given by $4\pi R_b^3 \rho_0 M_{\rm He}$.[12] These curves were usually used to investigate spectral features such as peak shift, line broadening, and line shape.

B. Deformed bubble model

The surface oscillation modes except the breathing modes have been neglected thus far, because a time-averaged bubble shape can be considered to be spherical for alkali atoms in the ground state $S_{1/2}$. It must be, however, noted that instantaneous oscillations of the bubble surface should not be restricted to only breathing modes, and even the lowest mode of such an oscillation causes a deformation of the bubble shape from a sphere. As suggested by Himbert *et al.*,[26] this instantaneous deformation leads to a lower symmetry of the interaction potential, which may remove the degeneracy of sublevels in the excited $P_{3/2}$ states (Jahn-Teller effect) and split the D_2 excitation line into two components. In this subsection, we first extend the SBM to the deformed bubble model (DBM). In particular, we will treat the deformation due to a quadrupole oscillation of bubble surface.

When we write R_S as the distance from the origin (alkali nucleus) to the bubble surface, the deformed bubble shape can be expressed by a spherical harmonics expansion as

$$R_S(R_0,\Theta,\Phi)=R_0+\sum_{L=1}^{\infty}\sum_{M=-L}^{L} R_{LM}Y_L^M(\Theta,\Phi), \quad (2.5)$$

where L runs generally from 1 to ∞ (the $L=0$ term is included in the R_0) and M is summed over from $-L$ to L.[19] The first term in Eq. (2.5) is the radius of a spherical bubble and the other terms represent the deformation from this sphere. The expansion coefficients R_{LM} can be considered to be small compared with R_0 in equilibrium for the alkali metal atom in the ground state $S_{1/2}$. The R_{LM} and the polar angles Θ and Φ are variables with respect to the same bubble-fixed coordinate system as in the SBM where the coordinate system of the center of mass of the spherical bubble has implicitly been used (namely, the origin is at the alkali nucleus). The $L=1$ terms in Eq. (2.5) represent the translation of the center of mass of bubble, so that they can be neglected in the present case.

We will restrict ourselves to the case of a quadrupole-deformed bubble:

$$R_S(R_0,\Theta,\Phi)=R_0+\sum_{M=-2}^{2} R_{2M}Y_2^M(\Theta,\Phi). \quad (2.6)$$

In previous studies concerning the deformation of the bubble shape, only the effect of axially symmetric oscillations ($R_{20}\neq 0$, $R_{2M}=0$ for $M\neq 0$) was taken into account.[5,8,12,16,18–20] This is physically incorrect in the case of the ground state, since there is no preferential direction for the deformation axis. All the fluctuations of the coefficients R_{2M} must be taken into account. In fact, model calculations using only one deformation parameter do not cause splitting profiles.[20,28] However, it is still difficult to treat directly the general case where there exist six independent parameters R_0 and R_{2M} ($M=-2,\ldots,2$). In order to reduce this difficulty, we transfer the coordinate system to the one whose three axes coincide with the principal axes of the deformed bubble. In this coordinate system, the deformed bubble shape can be written as[27]

$$R_S'(R_0,\Theta',\Phi')=R_0+R_{20}'Y_2^0(\Theta') + R_{22}'[Y_2^2(\Theta',\Phi')+Y_2^{-2}(\Theta',\Phi')]/\sqrt{2}, \quad (2.7)$$

where the angles Θ' and Φ' represent the polar angles and the coefficients labeled by primes denote those in this coordinates system. The origin of the system and R_0 are unchanged by this transformation. The original five degrees of freedom corresponding to the coefficients R_{2M} ($M=-2,\ldots,2$) are approximately separated into two parts: One is the two quadrupole oscillation modes of the bubble surface represented by the second and third terms in Eq. (2.7), and the other is the bubble rotation expressed by three Euler angles which were defined as the direction of the new coordinate system relative to that before transformation. We will show later that the energy of the bubble rotation can be neglected, because the bubble rotation can be considered to be almost stationary during a period of the surface oscillation. We choose the Z' axis as the quantization axis for the atomic wave functions. It must be noted that the potential $V_I(\mathbf{r},\mathbf{R})$ and the matrix elements of the total Hamiltonian H_E can be calculated in this coordinate system in the same manner as in the previous subsection, and the results obtained by the SBM calculation do not change by the coordinate transformation. Therefore, we will use the new coordinate system, omitting the primes hereafter.

The fundamental concepts of the DBM are about the same as those of the SBM, the only difference being the anisotropy in the configuration of surrounding liquid helium. By replacing R_0 in the SBM by R_S, the density distribution of the surrounding helium atoms in the DBM can be written as

$$\rho(R,R_S,\alpha)=\begin{cases}0, & \mathrm{R}<\mathrm{R_S},\\ \rho_0[1-\{1+\alpha(R-R_S)\}e^{-\alpha(R-R_S)}], & \mathrm{R_S}\leqslant \mathrm{R},\end{cases} \quad (2.8)$$

where ρ_0 is the pressure-dependent number density of liquid helium and $R_S(R_0,\Theta,\Phi)$ is given by Eq. (2.7). The two types of quadrupole oscillation modes represented by $R_{20}Y_2^0(\Theta)$ and $R_{22}[Y_2^2(\Theta,\Phi)+Y_2^{-2}(\Theta,\Phi)]/\sqrt{2}$ correspond to β and γ oscillations in the deformed nucleus theory, respectively.[27] The total Hamiltonian is obtained by substituting Eq. (2.8) into Eq. (2.1), and its diagonalization is made with the same atomic basis as in the SBM calculation. The summation over L in Eq. (2.1) depends on the atomic angular states involved.[21] For example, we use the S state and the first excited P states as atomic basis. In this case, the higher-order terms ($L\geqslant 3$) vanish. This is just the case of the quadrupole deformation. It can be considered that both breathing and quadrupole oscillation modes are induced si-

multaneously and independently by the zero-point fluctuations. R_0, R_{20}, and R_{22} are regarded as independent configuration coordinates.

The energy diagram associated with the excitation process is that for the equilibrium bubble configuration in the ground state $6S_{1/2}$. The bubble shape is determined by the coordinates (R_0, R_{20}, R_{22}) and the surface thickness parameter α. Since the quadrupole deformation is assumed to be small, the values of the parameter α and effective bubble radius R_b obtained by the SBM calculation can approximately be used even in the DBM calculation. In this case the surface energy and the pressure volume work are, respectively, given by[8]

$$E_{\rm surf}=\{4\pi R_b^2+4R_b^2(R_{20}^2+R_{22}^2)/R_0^2\}\sigma, \tag{2.9}$$

$$E_{\rm PV}=\{\tfrac{4}{3}\pi R_b^3+R_b^3(R_{20}^2+R_{22}^2)/R_0^2\}P. \tag{2.10}$$

The energy surfaces of the ground state $S_{1/2}$ and the first excited states $P_{1/2}$ and $P_{3/2}$ can be obtained by summing the eigenenergies of Hamiltonian H_E, $E_{\rm surf}$, $E_{\rm PV}$, and $E_{\rm VK}$, as changing R_0, R_{20}, and R_{22}.

III. NUMERICAL RESULTS AND DISCUSSION

A. Calculated energy surfaces

Here, we describe mainly the results of numerical calculations of the energy diagrams for the Cs bubble at SVP.

The treatment of multidimension configuration coordinate diagrams is a nontrivial work. We consider here the energy surfaces of an atomic bubble in the coordinates R_0, R_{20}, and R_{22}, at the moment of optical excitation. In this case, the configuration of surrounding helium atoms for the electronic ground state is essential to determine the excitation line shape. The vibrational coordinates R_0, R_{20}, and R_{22} distributed in the vicinity of the minimum of energy surfaces of the ground state $S_{1/2}$ are particularly important.

To visualize the physical mechanism of line splitting discussed in the next subsection, we schematically show in Fig. 2 the energy surfaces of the $6^2S_{1/2}$, $6^2P_{1/2}$, and $6^2P_{3/2}$ states of a Cs atom in the coordinates (R_{20},R_{22}) for R_0 = 11.375 a.u. This value of R_0 was obtained by minimizing the energy of the ground state $6^2S_{1/2}$ in the SBM and DBM calculations. As seen in Fig. 2, the energy surface of the $P_{3/2}$ state in the (R_{20},R_{22}) coordinates is split into two branches: upper and lower branches. On the contrary, such a splitting does not occur in the $P_{1/2}$ states. The energy surface of the $S_{1/2}$ states is regarded to be symmetrical for the rotation around the E axis in Fig. 2. Two branches of the $P_{3/2}$ states do not have such rotational symmetry. However, the rotational symmetry holds roughly in the region of R_{20} and R_{22} where the probability of the wave function of the vibronic ground state is mostly distributed ($0\leqslant\sqrt{R_{20}^2+R_{22}^2}\leqslant\sim 3.0$ a.u. in this case).

We regard the energy surfaces as the effective potentials for the quantized quadrupole oscillation modes of the bubble surface, similarly to the case of breathing modes in a spherical bubble. The effective mass $M_{\rm eff}^Q$ for the quadrupole oscillation modes is given by $R_b^3\rho_0 M_{\rm He}/3$.[20] By fitting the energy surface of the $S_{1/2}$ state to a two-dimensional harmonic potential, the wave functions of the vibronic states for the quadrupole oscillation can be easily obtained. The energy separation between the lowest two vibronic states in the electronic ground state $S_{1/2}$ is typically $\sim$9.6 K at SVP, which is much larger than the thermal energy in our experiment ($T\sim$1.6 K). Thus we can consider that the optical excitation transition occurs mostly from the vibronic ground state $\chi_{v=0}^Q$.

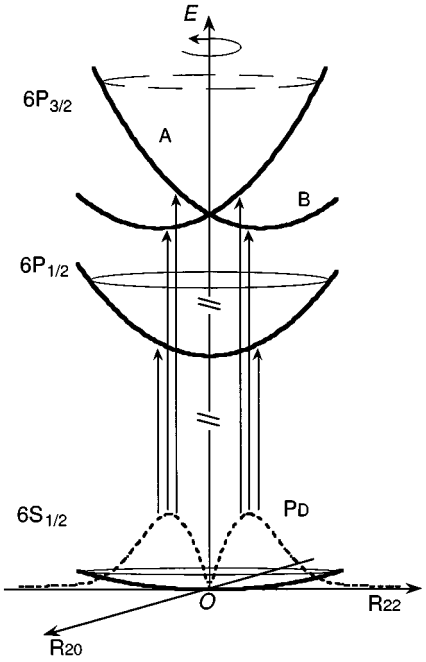

FIG. 2. Energy diagram of the Cs atomic bubble in the two-dimensional configuration coordinate, where R_{20} and R_{22} represent equivalent quadrupole oscillation modes. These energy surfaces are for the bubble in the ground $6S_{1/2}$ state and first excited states $6P_{1/2}$ and $6P_{3/2}$, in the case that R_0 is fixed to $R_{0\rm eq}$ (=11.375 a.u.) which gives the minimum energy of the ground state $6S_{1/2}$ at SVP. The quadrupole oscillation modes lift the degeneracy of the $P_{3/2}$ states and split the energy surfaces, while the energy surface of the $P_{1/2}$ state is not separated. The two branches of the $P_{3/2}$ energy surfaces do not have exactly a rotational symmetry around the Z axis and have a minima at $\sim$3.0 a.u. apart from the origin. The probability distribution P_D of the vibronic ground state in the electronic ground state $S_{1/2}$ is also shown by a dashed line, the maximum of which occurs at a distance of $\sim$1.2 a.u. from the origin. The arrows represent the D_1 and D_2 transitions, respectively.

We have not taken account of the rotational energy of the bubble in the above calculation. The rotational energy can be estimated roughly to be

$$E_{\rm rot}\sim\frac{\hbar^2}{M_I}, \tag{3.1}$$

where M_I is a moment of inertia of the bubble, given approximately by $\sim 4\pi R_b^5\rho_0 M_{\rm He}/3$. For the Cs bubble in the ground state $S_{1/2}$ at SVP (R_b = 13.785 a.u. and ρ_0 = 2.18 $\times 10^{22}$ cm^{-3}), we obtain the rotational frequency $\omega_{\rm rot}\sim 10^9$ sec^{-1}. Since $\omega_{\rm rot}$ is much smaller than the breathing oscillation frequency ($\omega_B\sim 5\times 10^{11}$ sec^{-1}) and the quadrupole oscillation frequency ($\omega_Q\sim 10^{12}$ sec^{-1}), the bubble rotation can be regarded to be adiabatic against bubble surface oscillations and the effect of rotational energy on the optical transition can be neglected. In addition, the change of the mo-

ment of inertia due to bubble surface oscillations is expected to be small, so that the rotation-vibration interaction is also negligible.

B. Interpretation of the line shape by the dynamic Jahn-Teller effect

Using the energy diagram in three-dimensional configuration coordinates (R_0, R_{20}, R_{22}), we obtained numerically the excitation line shape under the approximations as follows. We first fixed R_0 to the value of the equilibrium bubble radius $R_{0\mathrm{eq}}$ in the ground state $S_{1/2}$ and considered the energy surfaces in two-dimensional configuration coordinates (R_{20}, R_{22}) (see Fig. 2). According to the Franck-Condon approximation, the excitation spectrum was obtained by projecting the probability distribution P_D concerning the vibrational coordinates to the excited potential surfaces, as keeping constant the values of R_{20} and R_{22}. The probability P_D is calculated from the wave function of the vibronic ground state, $|\chi^Q_{v=0}| \propto \exp\{(-M^Q_{\mathrm{eff}}\omega_Q(R^2_{20}+R^2_{22})/2\hbar)\}$. Since two coordinates R_{20} and R_{22} should be treated equivalently and the energy surfaces have approximately rotational symmetry, P_D can be written as

$$P_D \propto \sqrt{R^2_{20}+R^2_{22}}\,|\chi^Q_{v=0}|^2, \tag{3.2}$$

where the factor $\sqrt{R^2_{20}+R^2_{22}}$ comes from the fact that P_D must be distributed in a two-dimensional (R_{20}, R_{22}) plane. Although $|\chi^Q_{v=0}|^2$ has a maximum at the origin, the maximum of P_D is displaced to a circle on the (R_{20}, R_{22}) plane with a radius given by $\sqrt{R^2_{20}+R^2_{22}} = \sqrt{\hbar/2M^Q_{\mathrm{eff}}\omega_Q}$, as shown by the dashed line in Fig. 2. The radius is actually distributed in a range 1.0–1.3 a.u., depending on the helium pressure. The twofold splitting of the D_2 excitation line is basically caused by the distribution of two possible resonant frequencies for the transitions from the ground state with $v = 0$ to the energy surfaces of the $P_{3/2}$ state, weighted by the probability distribution P_D. It is clear that no splitting structure appears in the D_1 excitation spectrum, as seen in Fig. 2. Thus we see that two quadrupole oscillation modes induced by zero-point fluctuations are found to be of great importance for the separation of the energy surfaces of the $P_{3/2}$ state and the resulting excitation line shape. In other words, it can be said that the dynamic Jahn-Teller effect plays an important role in the D_2 excitation.

There are two other important points to note in the calculation of the D_2 excitation spectra. First, there is no preferential direction of the principal Z axis for the bubble surface oscillations in the ground state $S_{1/2}$. Therefore, the angle between the electric field vector **E** of the linearly polarized excitation laser light and the bubble principal Z axis is distributed over all directions with equal probability. We calculated the electric dipole moment for transitions from the ground state $S_{1/2}$ to the two states of the excited $P_{3/2}$ state with different energy surfaces in the (R_{20}, R_{22}) configuration, averaging the angle between the direction of **E** and the Z axis. We obtained the transition probability to the lower and upper branches of energy surfaces by projecting vertically the probability distribution P_D, weighting the averaged square of electric dipole moment.

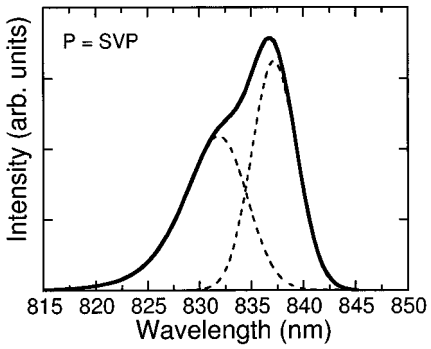

FIG. 3. Calculated shapes for the Cs-D_2 excitation spectra with the deformed bubble model (DBM) at SVP. The whole profiles (solid lines) are given by the superposition of broad and sharp components (dashed lines), which correspond, respectively, to transitions to the upper and lower branches of the twofold energy surfaces of the $P_{3/2}$ states.

Until now, we have considered only the quadrupole bubble deformation, with the bubble radius R_0 fixed to $R_{0\mathrm{eq}}$. As mentioned already, the breathing modes are independent of the quadrupole oscillation modes. Among the quantized breathing modes, only the lowest vibronic state $\chi^B_{v=0}$ in the electronic ground state $S_{1/2}$ is considered to be populated in equilibrium.[10] As shown in Fig. 1, a zero-point breathing oscillation distributes the bubble radius R_0 around $R_{0\mathrm{eq}}$, and it does not contribute to the line splitting, but solely to the broadening. This line broadening must not be ignored to obtain the whole line shape. This is the second point that we must take into account. To take account of the line broadening by the breathing oscillation, we calculated the excitation line profile for a particular value of R_0 in the way mentioned above, and integrated it over R_0, weighting the probability to find the bubble radius at R_0, i.e., the square of the wave function for the lowest breathing oscillation modes, $|\chi^B_{v=0}|^2$.

C. Comparison with experimental results

The calculated shapes of the Cs-D_2 excitation line at SVP and 20 atm of helium pressure are shown in Figs. 3 and 4, respectively. We can see that the calculated line (solid line) is given by the superposition of broad and sharp components shown by dashed lines. The difference in the shapes of these

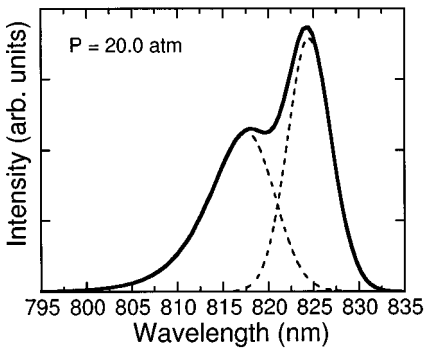

FIG. 4. Same as in Fig. 3, but for the case of 20 atm of helium pressure.

TABLE I. Theoretical and experimental values of center wavelengths, widths, ratios of relative intensities, and splitting intervals of two components of the Cs-D_2 excitation spectrum at helium pressure of the SVP and 20.0 atm. These theoretical values were obtained with the deformed bubble model (DBM). The observed line profiles were found to be well expressed by the sum of two Gaussian functions, from which the experimental values were obtained.

	Component I		Component II			Splitting interval
	Center (nm)	FWHM (nm)	Center (nm)	FWHM (nm)	Intesnity ratio I/II	(cm^{-1})
SVP						
Experiment	833.6	6.3	825.2	17.4	1.50	122.1
Theory	837.2	5.1	831.9	7.2	1.64	76.1
20.0 atm						
Experiment	819.2	9.4	808.8	16.4	1.49	157.0
Theory	824.6	5.7	817.5	10.4	1.62	105.3

two components comes from the different curvatures of the two energy surfaces of the $P_{3/2}$ states in the region of R_{20} and R_{22} giving the maximum of P_D, as seen in Fig. 2. Namely, the upper and lower energy surfaces in the vicinity of the maximum of P_D are steep and flat, respectively. This gives basically the difference in the shape and position of the two components, one being broad and located at the longer-wavelength side and the other being sharp at the shorter-wavelength side. The theoretical values associated with the two components of the D_2 line are shown in Table I, together with experimental values. The calculated line shapes, shown in Figs. 3 and 4, agree basically with those observed experimentally (see Fig. 5 in Ref. 10). Therefore, we can conclude that the doubly peaked profile of the D_2 excitation line can be attributed to the quadrupole deformation of the bubble shape and is explained as the dynamic Jahn-Teller effect. There exists, however, quantitatively, a discrepancy in the position, broadenings, and splitting of the two components of the D_2 line between theory and experiment. The theoretical splitting interval and broadening are about 65% of the experimental values, respectively. The pressure dependence of the calculated splitting interval is ~ 1.2 cm^{-1}/atm, which is smaller than the observed values (~ 1.6 cm^{-1}/atm). To remove these quantitative discrepancies, more precise calculations may be required.

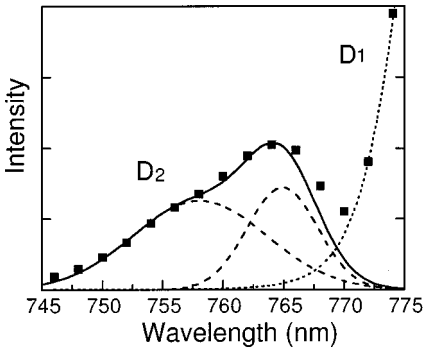

FIG. 5. Observed Rb-D_2 excitation spectra at SVP. Fitting the D_2 spectrum to the sum of two Gaussian curves after eliminating partially the overlap of the D_1 line shown by dotted line. The solid squares show the experimental results. The best-fit two components are shown by dashed lines and the solid line is a sum of the two dashed lines. The center wavelength and broadening (FWHM) of the sharper component were found to be 764.9 nm and 6.8 nm, respectively. The corresponding values of the other component were 758.1 nm and 13.0 nm. The resulting splitting interval was 117.3 cm^{-1}.

D. Volume constant condition

In the present model, the bubble shape parameters R_0, R_{20}, and R_{22} have been treated as independent variables. If the bubble deformation occurs under the conservation of bubble volume, i.e., $\delta V=0$, the surface energy and pressure volume work are rewritten as[20,27]

$$E_{\rm surf}=\{4\pi R_b^2+2R_b^2(R_{20}^2+R_{22}^2)/R_0^2\}\sigma, \tag{3.3}$$

$$E_{\rm PV}=\tfrac{4}{3}\pi R_b^3 P. \tag{3.4}$$

When the deformation is small, $E_{\rm surf}$ and $E_{\rm PV}$ given by the above equations are not so different from those given by Eqs. (2.9) and (2.10). However, R_0, R_{20}, and R_{22} are no longer independent variables.[27] In a high-helium-pressure region, the pressure volume work contributes largely to the total energy. In such a case, the breathing modes which always accompany the change of the bubble volume may be suppressed and quadrupole oscillation modes are considered to be dominant to determine the energy levels and modify the line shape and broadening from those calculated in the present work. A detailed study of this effect may be important to get quantitative agreement with experiment.

E. Case of a Rb atom

Figure 5 shows the magnification of the observed Rb-D_2 excitation line, which overlaps partially with the D_1 line. Looking at only the experimental results (solid squares), an obvious splitting of the D_2 line cannot be seen. However, as pointed out in our previous paper,[10] if we assume that the Rb-D_2 excitation line consists only of a single line, its linewidth [half width at half maximum (HWHM), typically ~ 440 cm^{-1}] is too broad compared with those of other ex-

citation spectra [full width at half maximum (FWHM), 120–170 cm^{-1}]. Thus, it may be natural to consider that the Rb-D_2 excitation line consists of two components as the Cs-D_2 line does. In fact, the Rb-D_2 line can be expressed as the sum of two Gaussian functions, as shown by the dashed lines in Fig. 5. The center wavelengths of the two components were found to be 764.9 nm and 758.1 nm, the splitting interval being therefore 117.3 cm^{-1}. We calculated the case of a Rb atom and obtained the doubly shaped profile of the D_2 excitation line, which has a shape similar to the Cs atom. However, as described above, the observed D_2 line does not have these well-resolved two components. We will discuss here the possible reasons for this. According to our DBM calculation, the Rb-D_2 excitation spectrum is, certainly, affected by the quadrupole deformation of the bubble surface. Our calculation shows that, if only the quadrupole oscillation modes exists, the resulting D_2 line shape must have a well-resolved splitting profile. However, there exists an effect of surrounding helium causing only the line broadening, resulting in the splitting profile being obscure. The breathing oscillation can be considered to be one of the most probable causes of broadening in this case. We believe that the splitting of the Rb-D_2 excitation line due to the dynamic Jahn-Teller effect may be masked by the large line broadening.[29] In fact, the observed splitting interval of the Rb-D_2 line was smaller than that of the Cs atom,[10] in spite of having the same line broadenings. Moreover, the small fine structure splitting $5P$ states of Rb causes a partial overlap of the D_1 and D_2 excitation lines, which may be an additional disturbance of the manifestation of spectral splitting.

There is an important point to be added. The D_2 line splitting, i.e., energy splitting of the $P_{3/2}$ state, may depend on the strength of the spin-orbit coupling relative to that of the asymmetrical vibronic coupling (Jahn-Teller effect). As pointed out by Fulton and Fitchen,[30] in the case that the spin-orbit coupling is much stronger than the asymmetrical vibronic coupling, a multiple splitting would occur in the absorption spectrum, and in the opposite case, only a single Gaussian band is predicted to appear. In fact, comparing the D_2 excitation lines of Ba^+ ions,[17] Cs and Rb atoms, which have fine-structure intervals of the first excited P states as 1691.2 cm^{-1}, 554.04 cm^{-1}, and 237.59 cm^{-1}, respectively, we see that the line splitting becomes smaller and unclearer in this order. To confirm this inference, a more accurate and quantitative calculation is required, particularly for the model of alkali-helium pair potentials.

IV. SUMMARY

The deformed atomic bubble model has been proposed and studied to clarify the physical mechanism for the structured profile of the D_2 excitation spectra of Rb and Cs atoms in He II which is beyond the description of the spherical the bubble model. In particular, we have restricted ourselves to the case of the oscillatory quadrupole deformation of the bubble surface induced by quantum zero-point fluctuations. The potential energy diagrams of a deformed bubble have been obtained using three configuration coordinates: One coordinate gives the bubble radius (breathing oscillation modes) and the other two give the bubble deformation (two quadrupole-oscillation-type modes) in the principal axis coordinate system of the deformed bubble. In the diagram, the lower symmetry in the interaction potential splits the energy surfaces of $P_{3/2}$ states into two branches. Franck-Condon transitions from the electronic ground state of the atomic bubble to these twofold energy surfaces lead to a splitting in the D_2 excitation spectrum, which is known as the dynamic Jahn-Teller effect.

After taking account of the additional line broadening by the breathing oscillation modes, the resulting line shape shows qualitative agreement with experimental results. Although there still exists a quantitative discrepancy with observed spectra, it can be said that the essential features of the line shape have been reproduced and the physical mechanism for the splitting has been explained in terms of the dynamic Jahn-Teller effect. Thus, it can be concluded that an anisotropic configuration of the surrounding liquid helium exists even for atoms in the ground state $S_{1/2}$ and produces the structured shape of the D_2 excitation line. It must be emphasized that the dynamic Jahn-Teller effect occurs not only in solids but also in liquids. A more quantitative treatment and model calculation are needed to understand the blurred D_2 profile for the Rb atom and to reproduce the line shape exactly.

ACKNOWLEDGMENTS

This work was partially supported by a Grant-in-Aid for Scientific Research (No. 07102011, 04554010) and SCAT. One of the authors (T.K.) acknowledges support from the Japan Society for the Promotion of Science for Japanese Young Scientists. He also thanks Dr. Akihiro Fujisaki for fruitful discussions, and the Laboratory for Elementary Particles and Nuclei at Kyoto University for permission to use the computer facilities.

*Present address: Laboratoire Kastler Brossel, Ecole Normale Supérieure, 24 rue Lhomond, 75231 Paris Cedex 05, France. Electronic address: kinosita@physique.ens.fr

[1] M. McCarty, Jr. and G. W. Robinson, Mol. Phys. **2**, 415 (1959); W. Weyhmann and F. M. Pipkin, Phys. Rev. **137**, A490 (1965); B. Meyer, J. Chem. Phys. **43**, 2986 (1965); H. Kuppelmaier, H. J. Stöckmann, A. Steinmetz, E. Görlach, and H. Ackermann, Phys. Lett. **98A**, 187 (1983).

[2] R. L. Mowery, J. C. Miller, E. R. Krausz, P. N. Schatz, S. M. Jacobs, and L. Andrews, J. Chem. Phys. **70**, 3920 (1979); J. C. Miller, R. L. Mowery, E. R. Krausz, S. M. Jacobs, H. M. Kim, P. N. Schatz, and L. Andrews, *ibid*. **74**, 6349 (1979); J. Hormes and J. Schiller, Chem. Phys. **74**, 433 (1983); P. A. Lund, D. Smith, S. M. Jacobs, and P. N. Schatz, J. Phys. Chem. **88**, 31 (1984); J. Rose, D. Smith, B. E. Williamson, P. N. Schatz, and M. C. M. O'Brien, *ibid*. **90**, 2608 (1986); C. Samet, J. L. Rose, P. N. Schatz, and M. C. M. O'Brien, Chem. Phys. Lett, **159**, 567 (1989).

[3] F. J. Soley and W. A. Fitzsimmons, Phys. Rev. Lett. **32**, 988 (1974).

[4] A. P. Hickman and N. F. Lane, Phys. Rev. Lett. **26**, 1216 (1971).
[5] A. P. Hickman, W. Steets, and N. F. Lane, Phys. Rev. B **12**, 3705 (1975).
[6] H. Bauer, M. Beau, A. Bernhardt, B. Friedl, and H. J. Reyher, Phys. Lett. A **137**, 217 (1989); S. I. Kanorsky, M. Arndt, R. Dziewior, A. Weis, and T. W. Hänsch, Phys. Rev. B **49**, 3645 (1994).
[7] H. Bauer, M. Beau, B. Friedl, C. Marchand, K. Miltner, and H. J. Reyer, Phys. Lett. A **146**, 134 (1990); G. zu. Putlitz, and M. R. Beau, in *Dye Lasers: 25 Years*, Topics in Applied Physics Vol. 70, edited by M. Stuke (Springer-Verlag, Berlin, 1992); J. H. M. Beijersbergen, Q. Hui, and M. Takami, Phys. Lett. A **181**, 393 (1993).
[8] S. I. Kanorsky, M. Arndt, R. Dziewior, A. Weis, and T. W. Hänsch, Phys. Rev. B **50**, 6296 (1994).
[9] A. Fujisaki, K. Sano, T. Kinoshita, Y. Takahashi, and T. Yabuzaki, Phys. Rev. Lett. **71**, 1039 (1993); Y. Takahashi, K. Sano, T. Kinoshita, and T. Yabuzaki, *ibid.* **71**, 1035 (1993).
[10] T. Kinoshita, K. Fukuda, Y. Takahashi, and T. Yabuzaki, Phys. Rev. A **52**, 2707 (1995).
[11] T. Kinoshita, K. Fukuda, Y. Takahashi, and T. Yabuzaki, Z. Phys. B **98**, 387 (1995).
[12] W. B. Fowler and D. L. Dexter, Phys. Rev. **176**, 337 (1968).
[13] J. Jortner, N. R. Kestner, S. A. Rice, and M. H. Cohen, J. Chem. Phys. **43**, 2614 (1965).
[14] K. Hiroike, N. R. Kestner, S. A. Rice, and J. Jortner, J. Chem. Phys. **43**, 2625 (1965).
[15] C. C. Grimes and G. Adams, Phys. Rev. B **41**, 6366 (1990); A. Ya. Parshin and S. V. Pereversev, Zh. Éksp. Teor. Fiz. **101**, 126 (1992) [Sov. Phys. JETP. **74**, 68 (1992)]; S. V. Pereversev and A. Ya. Parshin, Physica B **197**, 347 (1994); A. I. Golov and L. P. Mezhov-Deglin, Pis'ma Zh. Éksp. Teor. Fiz. **56**, 527 (1992) [JETP Lett. **56**, 514 (1992)].
[16] C. C. Grimes and G. Adams, Phys. Rev. B **45**, 2305 (1992).
[17] H. J. Reyher, H. Bauer, C. Huber, R. Mayer, A. Schafer, and A. Winnacker, Phys. Lett. A **115**, 238 (1986).
[18] E. P. Gross and H. Tung-Li, Phys. Rev. **170**, 190 (1968); V. Celli, M. H. Cohen, and M. J. Zuckerman, *ibid*. **173**, 253 (1968).
[19] B. Duvall and V. Celli, Phys. Rev. **180**, 276 (1969).
[20] P. B. Lerner, M. B. Chadwick, and I. M. Sokolov, J. Low Temp. Phys. **90**, 319 (1993).
[21] W. E. Baylis, J. Chem. Phys. **51**, 2665 (1969).
[22] J. Pascale and J. Vandeplanque, J. Chem. Phys. **60**, 2278 (1974).
[23] See, for example, J. Jortner, N. R. Kestner, S. A. Rice, and M. H. Cohen, in *Modern Quantum Chemistry-Istanbul Lectures*, edited by O. Sinanoglou (Academic Press, New York, 1966); N. R. Kestner, in *The Liquid State and Its Electrical Properties*, NATO Advanced Study Institute International Advanced Course, edited by E. E. Kuhnhardt, L. G. Christophorou, and L. H. Luessen (Plenum Press, New York, 1988), and references therein.
[24] F. Hermann and S. Skillman, *Atomic Structure Calculation* (Prentice-Hall, Englewood Cliffs, NJ, 1963).
[25] M. Iino, M. Suzuki, and A. J. Ikushima, J. Low Temp. Phys. **60**, 155 (1985).
[26] M. Himbert, A. Lezama, and J. Dupont-Roc, J. Phys. (Paris) **46**, 2009 (1985).
[27] A. Bohr and Mottelson, *Nuclear Structure* (Benjamin, Menlo Park, CA, 1975), Vol. II; N. A. Jelley, *Fundamentals of Nuclear Physics* (Cambridge University Press, Cambridge, England, 1990); J. M. Eisenberg and W. Greiner, *Nuclear Theory* (North-Holland, Amsterdam, 1975).
[28] Y. Toyozawa and M. Inoue, J. Phys. Soc. Jpn. **21**, 1663 (1966).
[29] I. Ya. Fugol, A. M. Ratner, and E. M. Yurtaeva, Phys. Status Solidi B **160**, 245 (1990).
[30] T. A. Fulton and D. B. Fitchen, Phys. Rev. **179**, 846 (1969).